Geophys. J. R. astr. Soc. (1987) **88**, 499–528

Crustal structure in the Society and Tuamotu Islands, French Polynesia

Jacques Talandier *Laboratoire de Géophysique, Commissariat à l'Energie Atomique, Boîte Postale 640, Papeete, Tahiti, French Polynesia*

Emile A. Okal *Department of Geological Sciences, Northwestern University, Evanston, Illinois 60201, USA*

Accepted 1986 July 10. Received 1986 June 24; in original form 1985 November 13

Summary. We present seismic investigations of the crustal structure of Tahiti (Society Islands), Rangiroa (Tuamotu Islands), and neighbouring areas. Records from a series of 96 explosions at the short-period stations of the Polynesian Seismic Network form a seismic refraction dataset from which we recover the crustal structures. The crust in the vicinity of Tahiti has the classic structure of 70 Myr-old ocean floor, and features an 8.8 km-thick crust (below sea floor) with a 7.64–8.25 km s^{-1} jump at the Mohorovičić (Moho) discontinuity. On the other hand, the Tuamotu plateau shows a very thick crust, reaching 31 km below sea floor, with a 6.83–8.10 km s^{-1} jump at the Moho. In addition, Rangiroa atoll itself features a 2 km-thick layer of slow material (3.3 km s^{-1}) which we interpret as limestone; comparable structures have been reported at Enewetak and Bikini.

We further use the short-period seismic arrays on Rangiroa and Tahiti to recover the slowness vectors, and, hence, the dispersion characteristics, of Rayleigh waves in the 15–40 s period range recorded from teleseismic events. Rayleigh dispersion under the Society Islands is compatible with published oceanic models of adequate age. We also use long-period records in the 20–90 s range for the path Rangiroa–Hao orientated along the Tuamotu plateau. The Rangiroa–Hao dispersion is slower than previously determined in neighbouring oceanic areas, and compatible with a crust 22–30 km thick under the Tuamotu plateau. Dispersion under Rangiroa is even slower, and requires a thicker (~35 km) crust. Any crust of standard thickness can be ruled out, as it leads to unacceptably low (< 3 km s^{-1}) crustal *S*-velocities.

These results are comparable to structures published for the Iceland–Færœ and Walvis Ridges, and confirm that the Tuamotus were formed on-ridge, in agreement with their very weak geoid signature.

Key words: seismic refraction, Rayleigh dispersion, Tuamotu plateau, South-Central Pacific

Introduction

The islands of French Polynesia, spread over approximately 5×10^6 km^2 in the South-Central Pacific, can be divided into five groups (see Fig. 1), and are generally interpreted as the remnants of Hawaiian-type island chains, each generated by one or more hotspots (e.g. Jarrard & Clague 1977). Among these, the Society Islands are the simplest, most studied, and best understood chain; they resemble most closely the Hawaiian Islands, with the present position of the hotspot located at the highly active seismic zone of Teahitia–Mehetia, 70 km east of Tahiti (Talandier & Okal 1984). To the east, the Gambier Islands are interpreted to be part of the Pitcairn chain, which can be traced westward through the atolls of Mururoa, Tematangi, Duke of Gloucester and Hereheretue. The southern (Austral) islands form a linear chain ending at the presently active Macdonald Seamount; however, they feature rapid variations both in their geochemical signatures (Grall *et al.* 1985) and in their thermomechanical relation to the lithospheric plate (Calmant & Cazenave 1986), so that their history must be far more complex than suggested by a simple hotspot model. To the north, the Marquesas are clearly the expression of a short-lived episode of young mid-plate volcanism (Fischer, McNutt & Shure 1986); difficulties persist when trying to extrapolate the location of the presumed hotspot, both at present and in the geological past. Finally, the structure of the Tuamotu Islands is more complex; they sit on a broad plateau, rising continuously to 2000 m below sea-level (b.s.l.), 300–500 km wide, and more than

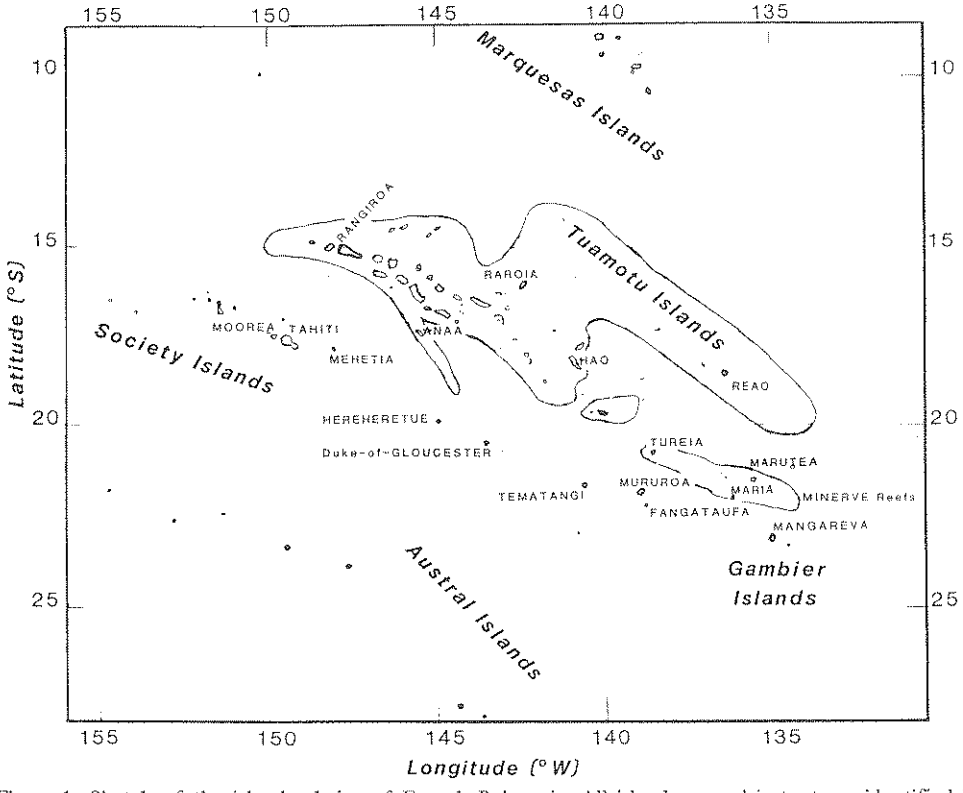

Figure 1. Sketch of the islands chains of French Polynesia. All islands named in text are identified by name on map, and their position highlighted. The thin trace represents the approximate boundary of the Tuamotu plateau.

1500 km long; all the islands are presently coral atolls. The only volcanic rocks ever dredged in the area come from the extreme north-western end of the plateau, where $^{40}Ar/^{39}Ar$ ages of 42 and 47 Myr were found (Schlanger *et al.* 1984); no volcanoes have ever been dredged or drilled from the island edifices, and thus only loose bounds exist on the age of either the plateau, or the island edifices themselves. East of longitude 143°W, the plateau breaks into a northern branch which remains a continuous bathymetric feature from Raroia to and past Reao, and a more discontinuous southern one (from Hao to Marutea and the Minerve reefs, north of the Gambier Islands). Although it represents a major bathymetry anomaly in the Central Pacific, the Tuamotu plateau shows only a very small geoid signature. On this basis, and following a number of reconstructions of plate motions since the Cretaceous, it has been proposed that the Tuamotu plateau was formed between 70 and 35 Myr by one or several 'on-ridge' hotspots, in a manner similar to the Iceland–Færœ plateau, or the Walvis Ridge in the South Atlantic. Constraints on the origin of the plateau, and possible models for its formation, can be found in Schlanger *et al.* (1976a, 1984), Pilger & Handschumacher (1981), Okal & Cazenave (1985) and Gordon & Henderson (1986). However, these models have not been confirmed by independent local investigations, and indeed very little geophysical work has been done regarding the structure of any of the atolls in the Tuamotus.

The purpose of the present paper is to report a series of seismic investigations into the upper crustal structures of the islands of Tahiti (Society), Rangiroa (Tuamotu), and neighbouring areas. Considerable information on the crustal structure of oceanic islands and plateaux can be obtained from seismic techniques (e.g. Woollard 1975; Hussong, Wipperman & Kroenke 1979). Alternatively, Chave (1979) used surface wave dispersion to propose crustal thickening under the Walvis Ridge. We present results of both a large seismic refraction campaign in the area, and Rayleigh wave dispersion studies in Rangiroa and along the Tuamotu plateau. We obtain crustal thicknesses of 13 km under Tahiti and 31 km under Rangiroa, in agreement with the fundamentally different histories of the two islands.

1 Seismic refraction experiments

The Réseau Sismique Polynésien (RSP) is a wide-aperture seismic network which has operated in French Polynesia since 1962 and has grown to 15 short-period and 5 long-period stations. A detailed description of its characteristics can be found in Talandier & Kuster (1976) and Okal *et al.* (1980). The stations relevant to the present study make up two sub-arrays, one on Tahiti and nearby Moorea in the Society Islands (AFR, PAE, PPT, PPN, TVO), and the other one on Rangiroa (PMO, TPT, RUV, VAH), the second-largest atoll in the Pacific, located at the north-western end of the Tuamotus, 350 km NNE of Tahiti (see Fig. 2).

DATASET

The seismic refraction dataset used in this study consists of the records of 96 explosions shot in the area delimited by Tahiti, Mehetia and Rangiroa. Following the 1981 volcanoseismic swarm at Mehetia (Talandier & Okal, 1984), and in order to obtain precise locations for its major events, a 66-shot seismic refraction campaign along four profiles was carried out during the period 1981 December–1982 March. We also include in the dataset the result of an 8-shot profile west and east of Rangiroa obtained in 1968, and of 8 explosions carried out in 1966 around the islands of Tahiti, Moorea and Mehetia. Finally, the local structures of both Tahiti and Rangiroa were obtained from explosions fired in the lagoons of Rangiroa

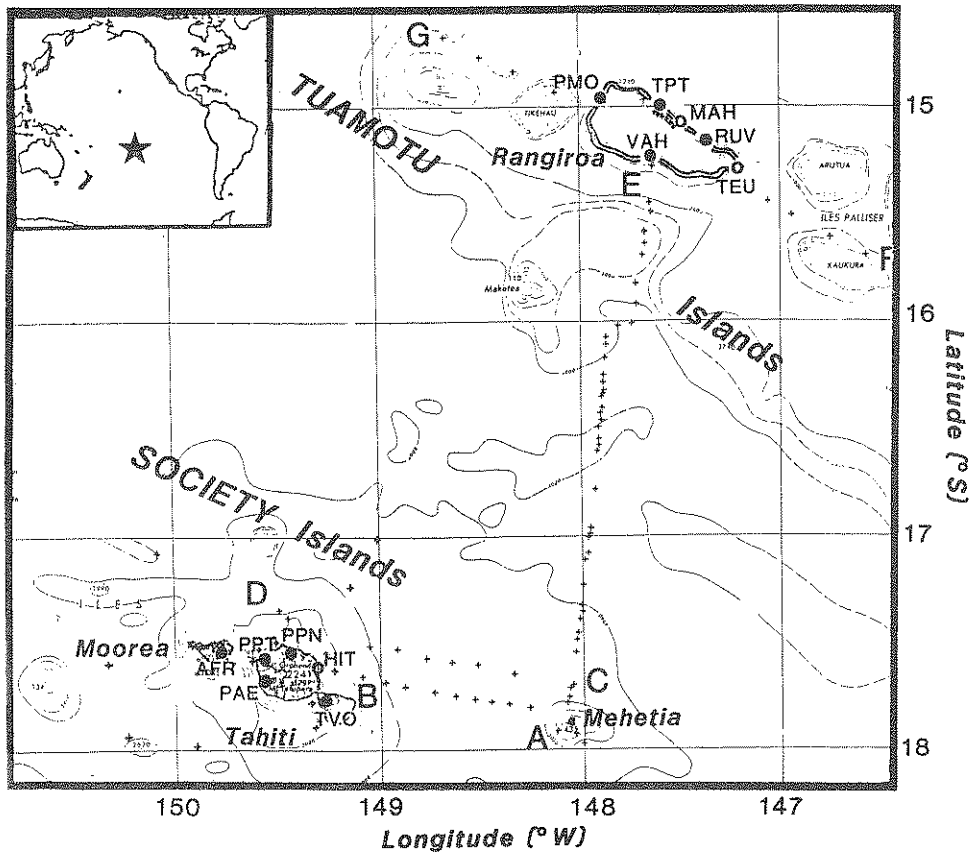

Figure 2. Map of the Tahiti–Rangiroa area, French Polynesia, superimposed on bathymetry from Institut Géographique National (1969). Inset shows position inside Pacific Ocean. The islands relevant to this study are outlined. Permanent seismic stations are shown as full circles (with 3-letter code); temporary ones as open circles. The locations of seismic refraction shots are shown as individual + signs. See Appendix and text for complete description of profiles.

in 1982 (7 shots) and of Tahiti and Moorea (7 shots) in 1963–64. Fig. 2 summarizes the layout of the refraction experiments, while Appendix 1 gives the details of sources used, timing methods, and data transmission and storage. Whenever possible, we used both first and later arrivals. The latter are not always observed; also, as discussed below, some of the slower arrivals correspond most probably to propagation in the form of surface waves, and could not be readily interpreted.

All explosions were recorded at the nine permanent RSP stations listed above; in addition three temporary stations were used; TEU at the south-eastern tip of Rangiroa in 1968, MAH on its north-eastern coast in June 1982, and HIT on the eastern shore of Tahiti during the shooting of profile AB.

DATA PROCESSING

Our purpose is to obtain crustal models for the oceanic areas neighbouring Tahiti and Rangiroa, and to use the lagoon surveys to modify the top portions of these models in order to describe the shallow structures under the islands.

The use of permanent island stations in a seismic refraction experiment has a number of advantages over the more classical recording at sea: in addition to simplifying logistics and reducing costs, it makes use of stations with improved detection capabilities, thus extending the range of the experiment; also, it allows the recognition of anomalous behaviour at individual stations and the definition of station corrections, which can then become a permanent part of regional earthquake location routines. On the other hand, using island stations as recording sites implies that the source and receiver structures will be *a priori* different, an additional complexity which must be carefully accounted for when interpreting the data.

Because of the configuration of the experiment, no record sections are obtained. In particular, distances sampled by the source-station layouts are not regularly spaced. While in principle, it could be possible to make artificial record sections by pasting individual records together (leading to a 'common receiver gather'), the need to use different stations, with different station corrections, would make the exercise futile.

Ocean corrections

A further problem arises from the variation of the depth of the oceanic column under the various source sites. Following Furumoto *et al.* (1968, 1971), we assume that a variation $\delta d = d - d_0$ of the depth to the ocean floor does not influence sediment thickness, and is totally taken up by a simultaneous variation $-\delta d = d_0 - d$ of the basaltic layer ['Layer 2' in Raitt's (1963) model]. This assumption does not lead to isostatic compensation of the structures; we note however that Tahiti and the nearby seamounts are *not* compensated. This crude model, which has been used in the Hawaiian Islands is justified *a posteriori* by the fits to Layer 2 hodochrones. According to this model, we compute a bathymetry correction c_{ocean} for each type of wave, once a preliminary model is known. Specifically, for a wave bottoming in or above the basaltic layer, the correction is given by $c_{ocean} = c_0$ with

$$c_0 = d\sqrt{1/V_0^2 - 1/V_i^2}, \tag{1}$$

where V_i is the velocity in the layer i where the ray bottoms, and $V_0 = 1.5$ km s^{-1} in the oceanic column. For a wave bottoming below the basaltic layer, $c_{ocean} = c_0 + c_2$ with c_0 given by (1) and

$$c_2 = (d_0 - d)\sqrt{1/V_2^2 - 1/V_i^2}, \tag{2}$$

where V_2 is the velocity in the basaltic Layer 2. Note that the estimation of these bathymetry corrections is independent of layer *thicknesses*. We use a reference depth $d_0 = 4$ km, and the preliminary structure listed in Table 1. It was found that a second set of bathymetry

Table 1. Preliminary model used for bathymetric corrections.

Layer	Structural Nature	*P*-wave Velocity (km/s)
0	Ocean	1.50
1	Sediments	2.20
2	Basalt	4.80
3	Gabbro	6.80
4	Mantle	8.20

corrections, run after obtaining our crustal structures, did not alter the final models significantly. Subtracting the corrections c_{ocean} from the arrival times recorded at the stations has the effect of moving the source to the floor of a reference ocean of depth $d_0 = 4$ km.

Stations corrections

For mantle (P_n) arrivals for which a sufficiently large dataset exists, station corrections were defined as the mean residual of the data points pertaining to the individual station, with respect to the subarray regression. These values are listed in Table 2; the correction consists of subtracting them from the experimental times. They can be attributed to variations in local structure in the immediate vicinity of the receivers. In the case of Tahiti, and

Table 2. Station corrections applied to P_n segments.

Station Code	Correction (s)
AFR	-0.05
PAE	-0.01
PPT	+0.07
PPN	-0.12
TVO	+0.07
HIT	-0.17
PMO	-0.01
VAH	0.00
TPT	-0.06
RUV	+0.14

significantly, the positive corrections correspond to stations located at altitudes of 250 m (PPT) and 620 m (TVO). New regressions were obtained after applying the corrections. These station corrections have also been made an integral part of regional earthquake location routines using the RSP network.

RESULTS

Fig. 3 shows the hodochrones of arrivals at the Tahiti and Rangiroa stations. The data are in general agreement with the classic model of three layers over a half-space (Raitt 1963). Because of its simplicity, we will interpret our dataset within this framework; in particular, we do not seek to represent our data with models featuring continuous gradients, which could also provide legitimate interpretations of the same dataset.

We obtained the velocities in the various layers as the inverse of the slownesses resulting from linear regression of the relevant segments of the hodochrones. Table 3 gives the values of layer velocities and time intersects for the mantle and crustal layers.

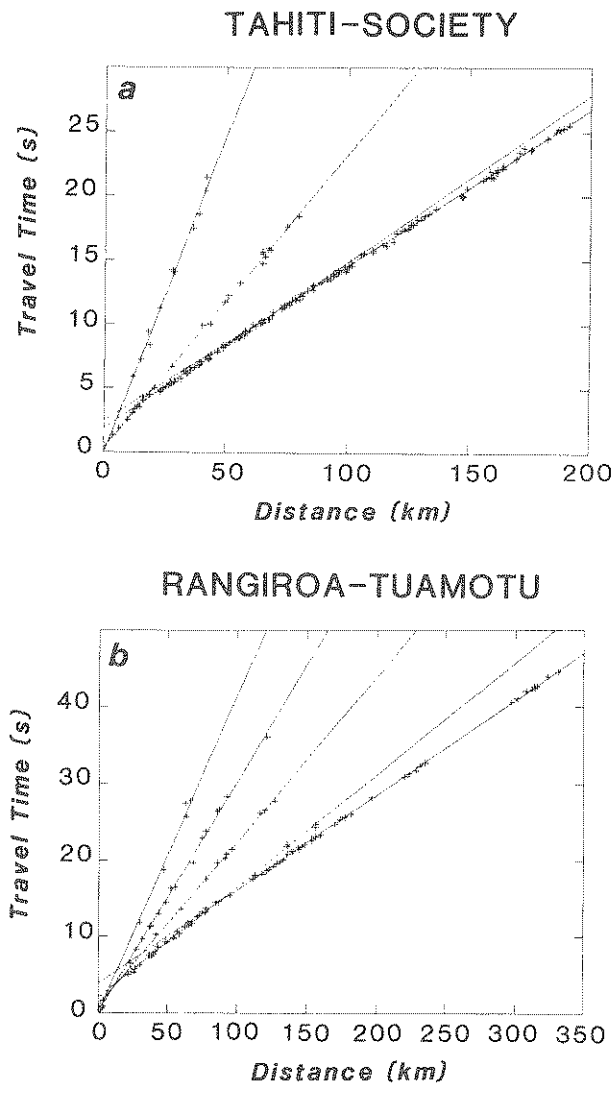

Figure 3. Seismic refraction datasets at the Tahiti (top; a) and Rangiroa (bottom; b) subarrays. Plus signs (+) represent the individual arrivals, and the oblique lines are the regressed linear travel times in each layer. See text and following figures for details.

Tahiti and Society area

In the case of mantle waves (Layer 4 – P_n) propagating to Tahiti, we considered profiles AB, CD, AE, and the local shots in 1963–64, both separately and as a whole, without noticing significant differences. The final regression used 82 data points and is shown on Fig. 4(a).

In the case of the presumably gabbroic Layer 3, we similarly carried out several regressions along individual profiles, without noticing differences; the final regression uses all 56 data (Fig. 4b). For the (basaltic) Layer 2, we use both first and later arrivals; we ran regressions both with and without data from the shallowest explosions at sea and in the lagoons, resulting in no significant differences; this confirms the validity of our bathymetry corrections and related hypotheses.

Table 3. Least-squares fits to travel-time data in each layer.

Layer	Structural Nature	Number of points used	Velocity (km/s)	Intercept (s)	Average thickness (km)
			Tahiti and Society		
1	Sediments		1.90	0.0	0.36
2	Basalt	28	4.37 ± 0.04	0.34 ± 0.09	3.84
3	Gabbro	56	7.68 ± 0.07	1.81 ± 0.06	6.13
4	Mantle	82	8.25 ± 0.03	2.44 ± 0.06	
			Rangiroa and Tuamotus		
1(*)	Sediments	7	1.90	0.0	1.05
1'(†)	Limestone	24	3.30 ±0.03	0.02	2.0
2	Basalts	25	4.65 ± 0.08	0.93 ± 0.29	2.87
3	Gabbro	58	6.85 ± 0.04	1.97 ± 0.07	24.51
4	Mantle	43	8.10 ± 0.02	5.92 ± 0.1	

* Oceanic (plateau) area only.
† Rangiroa (atoll) area only.

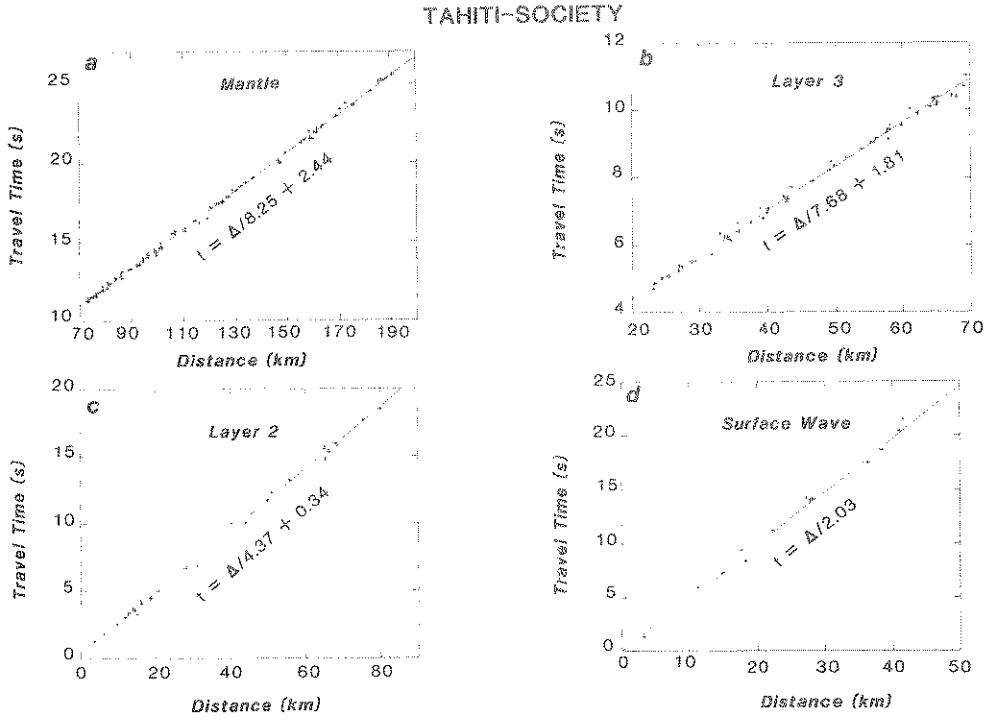

Figure 4. Regressed data for arrivals at the Tahiti stations. Each frame (a, b, or c) corresponds to rays having bottomed in the corresponding layer (Mantle, 3, or 2). The oblique lines are the results of the least-squares fits to the data. In the case of frame d, a surface wave is probably involved.

For the (sedimentary) Layer 1, we use first and later arrivals from both lagoon and ocean shots. As shown in Fig. 4(d), the two datasets are indistinguishable. However, these arrivals are of a characteristically lower frequency; their efficient propagation to large distances (40 km) argues against a typical Layer 1 *P*-wave. It is also improbable that these arrivals represent shear waves propagating in a deeper layer (e.g. Layer 2 shear waves), since they should exhibit a non-zero time intercept. Rather, we interpret these arrivals as corresponding to a surface-wave type of propagation, sampling both Layers 1 and 2.

Rangiroa and Tuamotu Plateau

In the case of Rangiroa, we used primarily profiles AE and FG, with a few additional data points from profiles AB and CD, recorded as P_n at station PMO. The seven lagoon shots were used to retrieve the shallow (sedimentary and limestone) structure of the island. Hodochrones are shown in Fig. 3(b). The most interesting feature in this dataset is the incompatibility of the fastest segments of the hodochrones for the two profiles AE and FG: separate regressions give velocities of 8.10 km s^{-1} (AE; north–south) and 6.85 km s^{-1} (FG; east–west) (see Fig. 5). It is unlikely that such a large discrepancy (18 per cent) could be due to azimuthal anisotropy: the typical amount of anisotropy in oceanic P_n is ± 2 per cent

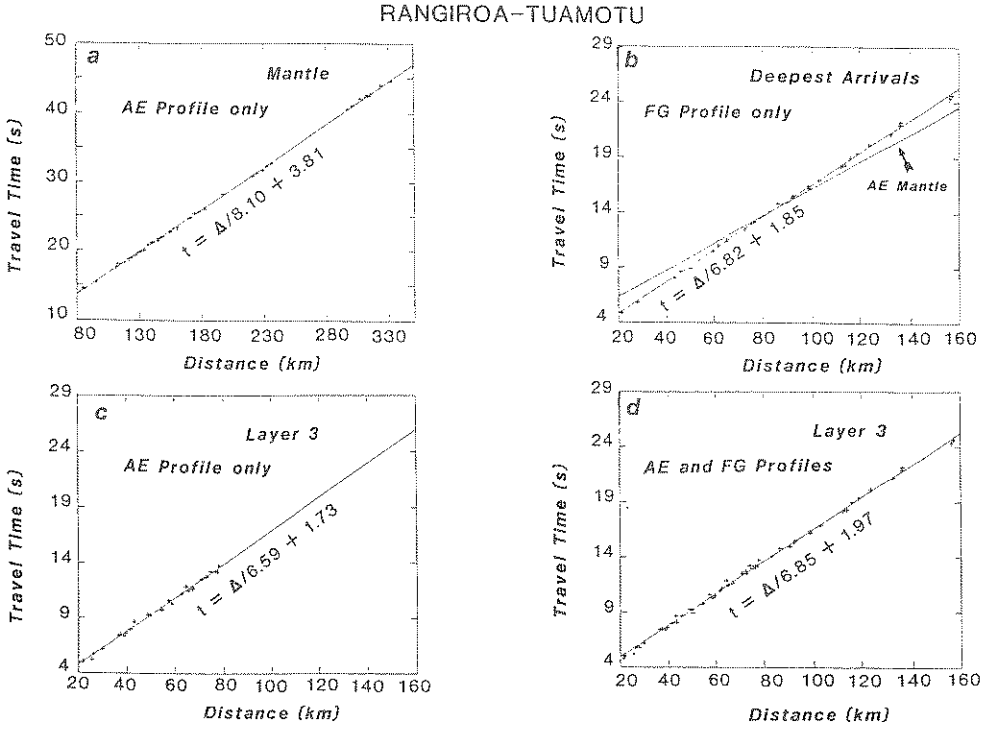

Figure 5. Regressed data for the mantle and Layer 3 arrivals at the Rangiroa array. The oblique lines are the results of least-squares fits to the various datasets. Frame (a) corresponds to mantle rays recorded from shots along profile AE (see Fig. 2); frame (b) shows that the deepest arrivals along profile FG are incompatible with the mantle rays from AE (reproduced as the dashed line on b), but, rather, similar to the Layer 3 arrivals along AE. Frame (d) shows the regression of the combined dataset of Layer 3 rays from AE and FG.

(Morris, Raitt & Shore, Jr. 1969; Talandier & Bouchon 1979), an order of magnitude less than found here; nor can it be reconciled through any reasonable dipping of the structures. Rather, we note that the velocity for Layer 3 along the north–south profile is in close agreement with the fastest east–west velocities. We therefore interpret east–west arrivals at distances as great as 150 km as still bottoming in Layer 3; P_n fails to materialize along the east–west profile, even at distances of more than 150 km, while it shows up clearly on the north–south profile at distances of 80 km or more. This suggests that the Mohorovičić (Moho) discontinuity is considerably deeper under the plateau, sampled exclusively by the rays from the east–west profile, than in the Society crustal model described above, where rays of the north–south profile originate.

The 43 P_n data points from the north–south profile alone can be regressed as $t = \Delta/(8.10 \pm 0.02) + (3.81 \pm 0.06)$ (t in seconds and Δ in km). Our modelling in Tahiti and the Society Islands can be used to compute a crustal correction for a source on the ocean floor in the Society area $\delta t_{Soc} = 0.85$ s. We use this value to compute what would be the time intercept of a hypothetical P_n propagating fully in the Tuamotu structure; this value, which is simply $[2 \times (3.81 - 0.85) = 5.92$ s] is included in Table 3 and will be used later to compute the layer thicknesses under the Tuamotus. It predicts emergence of P_n as the first arrival at a distance of 177 km, beyond the maximum range of the east–west profile FG.

The velocity of Layer 3 is found to be slightly lower (6.59 km s^{-1}) along the north–

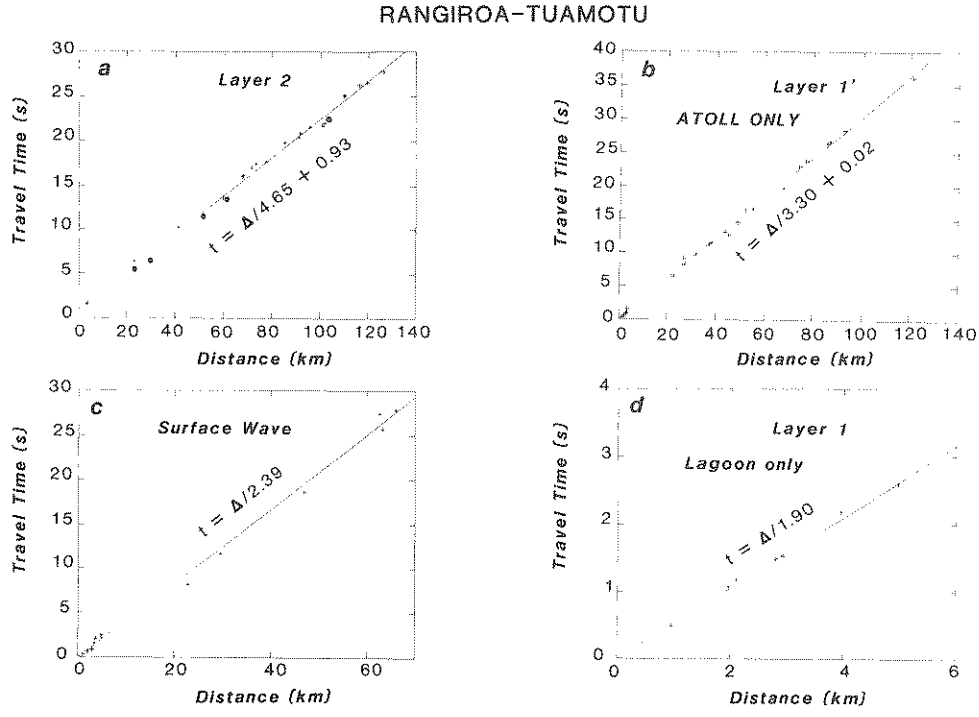

Figure 6. Regressed data for the Layer 2 and shallower arrivals at the Rangiroa array. The oblique lines are the results of least-squares fits to the various datasets. (a) Layer 2 arrivals; the plus signs (+) correspond to data from the north–south (AE) profile, the dots (•) to data from the east–west (FG) one, (b) Layer 1′ (limestone) arrivals, observed only for the east–west rays propagating in the atoll structure; (c) Arrivals from sources in the open ocean, probably involving surface wave propagation; (d) Layer 1 arrivals in the lagoon.

south profile than along the east–west one. This 3.5 per cent discrepancy can be interpreted as due to the dipping of the structure expected along the southern flank of the Tuamotu plateau.

An interesting structure in the Rangiroa data, absent from the Tahiti, Society and Tuamotu profiles, is a slow arrival at distances of 20–85 km (Fig. 6b), corresponding to a velocity of 3.3 km s^{-1}, which we interpret as propagation in a thick limestone layer (1′).

As in the case of Tahiti and the Society area, shots from profile FG evidence a low-frequency wave, with a speed of approximately 2.4 km s^{-1}, propagating up to 65 km. This velocity is difficult to reconcile with typical Layer 1 values; it most probably again corresponds to a surface-wave type of propagation (Fig. 6c). Inside the lagoon itself, first arrivals at distances of less than 6 km constrain the Layer 1 velocity to 1.90 km s^{-1} (Fig. 6d), and a low-frequency surface wave is found to propagate in the lagoon at velocities of 1.44 km s^{-1}, presumably in the shallowest parts of the atoll structure or in strong interaction with the water layer.

INTERPRETATION

Layer thicknesses can be readily obtained from the data in Table 3, by using standard refraction methodology. They are listed as the last columns in Table 3. In the case of Tahiti and the Society area, where we have no adequate Layer 1 arrivals, we use a Layer 1 velocity similar to that found in Rangiroa (1.9 km s^{-1}); it was found that this value has only minimal influence on the final structure. With the exception of the lagoon shots (used only to determine the velocities of Layers 1), all sources are at sea, and all receivers on the island edifices, which have an *a priori* different structure. Thus, the thicknesses in Table 3 represent a structure *averaging* the island edifice and the ocean nearby. In order to further separate the two, we make the following assumptions:

1. Seismic velocities are identical in layers of similar structure (e.g. Layer 2) below the island and nearby ocean;

2. Layering is everywhere horizontal (a necessary assumption in the absence of reverse profiling, and probably a correct one, except possibly at the southern flank of the Tuamotu plateau); and finally

3. The only difference in structure represents the filling of the standard 4 km deep oceanic water column by the basaltic layer.

Under these assumptions, we obtain the island and oceanic thicknesses of Layer 2 by adding and subtracting 2 km to the average thicknesses from Table 3.

A further complexity arises from the limestone layer (1′) at Rangiroa. There exists a trade-off between the thicknesses of the sedimentary layer (1) in the oceanic structure h_s, and of the limestone cap in the atoll h_c, which must simply satisfy:

$$h_c \sqrt{1/V_c^2 - 1/V_2^2} + h_s \sqrt{1/V_s^2 - 1/V_2^2} = 0.93 \text{ s}. \quad (3)$$

Sediment thicknesses greater than 1.2 km are improbable, and therefore, a limestone cap at least 2 km thick is required under Rangiroa. Its precise thickness cannot, however, be further constrained. Finally, the difference in thickness of the basaltic layers between Rangiroa and the Tuamotu plateau is taken as 2 km (rather than 4) to reflect the shallower bathymetry along the Tuamotu plateau.

The final models are listed in Table 4, and sketched on Fig. 7. In summary, the ocean near Tahiti is a classic example of oceanic crust. In particular, it is not fundamentally different from sections obtained in the vicinity of Hawaii, whose lithospheric age is

Table 4. Final crustal models.

Layer	Structural Nature	Velocity (km/s)	Thickness (km)	Total Depth (km)
		Tahiti (Island)		
1	Sediments	1.9	0.4	0.4
2	Basalts	4.37	5.8	6.2
3	Gabbro	7.64	6.1	12.3
4	Mantle	8.25	--	
		Society area (Ocean)		
0	Ocean	1.5	4.0	4.0
1	Sediments	1.9	0.4	4.4
2	Basalts	4.37	1.8	6.2
3	Gabbro	7.64	6.1	12.3
4	Mantle	8.25	--	
		Rangiroa (Atoll)		
0	Lagoon	1.5	0.03	0.03
1'	Limestone	3.3	2.0	2.0
2	Basalts	4.65	4.8	6.8
3	Gabbro	6.83	24.5	31.3
4	Mantle	8.10	--	
		Tuamotus (Plateau)		
0	Ocean	1.5	2.0	2.0
1	Sediments	1.9	1.1	3.1
2	Basalts	4.65	2.8	5.9
3	Gabbro	6.83	24.5	30.4
4	Mantle	8.10	--	

comparable (Furumoto *et al.* 1971). The seismic structure under Rangiroa features an anomalously thick crust (about 31 km), with a limestone cap at least 2 km thick.

2 Surface wave analysis

INTRODUCTION

The most important feature revealed by the refraction experiments is the thick crust under Rangiroa and the Tuamotu plateau. Our purpose in this section is to use Rayleigh wave

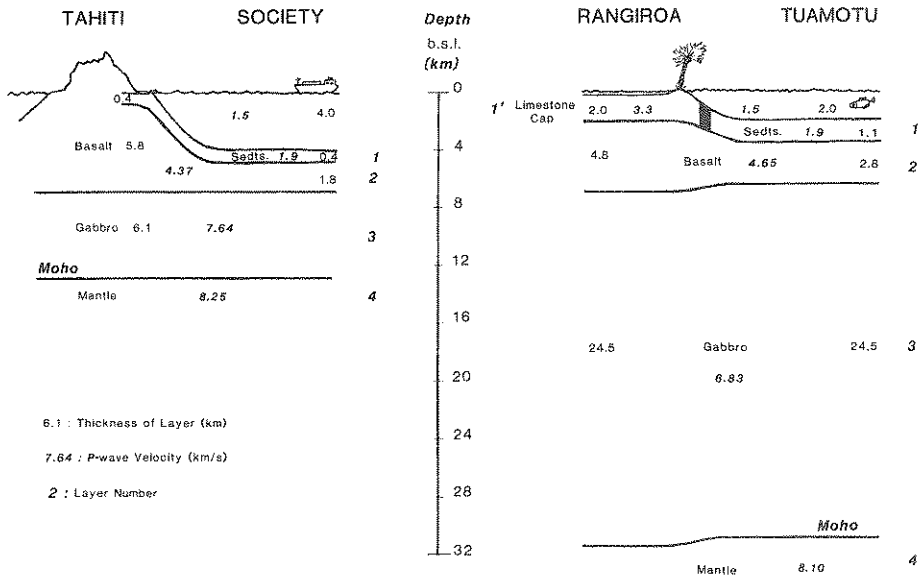

Figure 7. Cartoons summarizing the results of the seismic refraction experiments. The 'barrier' in the sedimentary layer under the Tuamotus emphasizes the difference in nature between Layers 1 (plateau) and 1′ (atoll). The cartoons have no horizontal scale.

dispersion across the structure to confirm this result. In the 20–30 s period range, and for Poisson solids, a 30 km crust is expected to induce Rayleigh wave phase velocities as much as 0.25 km s^{-1} slower than for a typical oceanic model, such as the one derived in the Society Islands.

In a previous study (Okal & Talandier 1980; hereafter Paper I), we used Rayleigh wave dispersion over the whole Polynesian array to confirm the local applicability of models of crust and upper mantle structure such as those of Mitchell & Yu (1980), obtained from Pacific-wide regionalization and pure-pathing; we also confirmed the existence of azimuthal anisotropy. As part of that study, we investigated the dispersion of Rayleigh waves along the path TPT–RKT, stretching 1600 km along the general orientation of the Tuamotu plateau, and found it significantly (~0.15 km s^{-1}) *faster* than average. We pointed out in Paper I that this path is not representative of typical oceanic lithosphere because of the presence of the island plateau, and refrained from using it in our discussion of dispersion anisotropy. However, it cannot be taken to simply represent the plateau structure either, since the path is inherently heterogeneous, and some of the rays used in Paper I actually missed the plateau structure almost entirely. We present below a detailed correction to this part of Paper I. Our scope in the present study is to concentrate on the clearly anomalous Tuamotu structure in more detail.

METHODOLOGY

In order to investigate the Tuamotu plateau, we use the two-station method between long-period stations at Tiputa, Rangiroa (TPT) and Otepa, Hao (OTP), 803 km to the south-east. We also use the station at Rikitea (RKT), on the island of Mangareva, Gambier, to correct and refine the original investigation in Paper I. We refer to Paper I and previous publications for a description of the classic two-station methodology. We use two sets of earthquakes,

one aligned nearly perfectly with TPT and OTP, the other with OTP and RKT. Their intermediate magnitudes are sufficient to provide enough energy in the seismograms, but prevent clipping of the analogue records at Otepa and Rikitea.

Since there exists only one long-period station on Rangiroa, we investigate the local structure of the atoll by extracting the long-period signal from digital records at the four short-period stations (see Fig. 2). This procedure was originally proposed by Press (1956) and applied in Southern California by Alexander (1963), and later Hadley & Kanamori (1979). As noted by these authors, a major problem arises in that the structures studied are comparable in size to the seismic wavelengths used, resulting in non-geometrical propagation. Fortunately, the presence of more than two stations allows the determination of a best-fitting two-dimensional horizontal wave vector $\mathbf{k}$ across the array at each frequency, from which both the azimuth of arrival ζ and the phase velocity C of the Rayleigh wave train can be retrieved. Specifically, at each angular frequency ω, and for a set of J stations, we extract the phases ϕ_j at each station and determine the vector $\mathbf{k}$ which minimizes

$$\sum_{j=1}^{J} (\phi_j - \mathbf{k} \cdot \mathbf{x}_j)^2, \tag{4}$$

where $\mathbf{x}_j$ is the radius vector from the centroid of the array to station j. Then ζ is simply the argument of $-\mathbf{k}$, and $C = \omega/k$. The only problem resides in the $2N\pi$ indeterminacy of the phases ϕ_j, which must be solved by trial and error; due to the small size of the array as compared with the typical wavelengths, there can be no ambiguity in N.

In order to more directly compare the structures under Tahiti and Rangiroa, we applied a similar procedure to the Tahiti–Moorea subarray of the RSP network; however, because of the even smaller size and flatter shape of the network, we could obtain only a few data points, mostly limited to the 15–20 s period range.

Finally, and considering the relatively high frequencies involved, it was evident that

Table 5. List of stations used in surface wave studies.

Code	Name	Island	Region	Latitude (°S)	Longitude (°W)	Nature
TPT	Tiputa	Rangiroa	Tuamotu	14.98	147.62	Short-Period
PMO	Pomariorio	Rangiroa	Tuamotu	15.00	147.90	Short-Period
VAH	Vaihoa	Rangiroa	Tuamotu	15.24	147.63	Short-Period
RUV	Rauvai	Rangiroa	Tuamotu	15.19	147.38	Short-Period
AFR	Afareaitu	Moorea	Society	17.54	149.78	Short-Period
PAE	Paea	Tahiti	Society	17.66	149.58	Short-Period
PPT	Pamatai	Tahiti	Society	17.57	149.58	Short-Period
PPN	Papenoo	Tahiti	Society	17.53	149.43	Short-Period
TVO	Taravao	Tahiti	Society	17.78	149.25	Short-Period
TPT	Tiputa	Rangiroa	Tuamotu	14.98	147.62	Long-Period
OTP	Otepa	Hao	Tuamotu	18.17	140.86	Long-Period
RKT	Rikitea	Mangareva	Gambier	23.12	134.97	Long-Period

anelasticity corrections (Kanamori & Anderson 1977) were not warranted, since they would have amounted to less than the uncertainty in the data.

RESULTS

Tables 5 and 6 list the coordinates of stations and epicentral information for earthquakes used in this study. We refer to Paper I for similar details concerning the data used in that study.

Subarray study

Some typical short-period seismograms recorded from truly large earthquakes at the Rangiroa subarray are shown on Fig. 8. At the frequencies involved in this study, which are typically outside the operating band of the seismometers, the instruments operate as accelerometers; since the sensor is itself velocity sensitive, the resulting signal is the third derivative of the vertical ground motion d^3z/dt^3, and the phase response can be predicted to be exactly $3\pi/2$. The reliability of the instrument response, and in particular its possible variation across the array, was checked in two ways: first we used several events arriving at different azimuths; the compatibility of the phase velocities thus obtained proves that any differences in phase response are not significant. Second, we compared records obtained at station TPT from short- and long-period instruments respectively: the identity of the ground motions recovered by deconvolving the systems' responses proved the reliability of the method.

The assessment of uncertainties and errors in two-station and other spatial filtering techniques has traditionally been difficult; following several authors (Forsyth 1975; Okal 1977; Yu & Mitchell 1979; Paper I), we use an uncertainty corresponding to twice the digitizing interval (0.10 s), or about ± 0.05 km s^{-1} on C in Rangiroa, and ± 0.06 km s^{-1} in the case of the smaller aperture Tahiti network. This is much larger than for typical Rayleigh wave studies (e.g. Paper I), but should be expected given the very small size of the network; indeed this precision is the same as claimed by Hadley & Kanamori (1979) for their California study. In the case of the TPT–OTP path, we used a 1 s sampling rate, and an 800 km path, resulting in an uncertainty of only 0.03 km s^{-1}.

Table 6. Earthquakes used in the surface wave study.

Event Number (*)	Date Y M D	Origin Time UT	Epicenter (°N)	Epicenter (°E)	Region	Magnitude M_s	Stations used
20	1978 05 26	23:58 22 0	24 274	142.661	Volcano Is	6 8	TPT, OTP,RKT
21	1978 05 29	17 20 29.4	-44.87	-79 60	Chile Ridge	6 0	OTP,RKT
22	1978 08 03	18:11 17.1	-26 513	-70.544	Chile	7 0	TPT, OTP, RKT
23	1979 02 20	06 32:32 2	40 232	143 703	No Honshu	6 4	OTP,RKT
24	1978 11 29	19 52.47.6	16.010	-96 591	Mexico	7 7	TPT, PMO, RUV, VAH
25	1980 07 17	19 42.23.2	-12.525	165.916	Santa Cruz	7 9	TPT, PMO, VAH, AFR, PPT, PAE, PPN, TVO
26	1983 05 26	02:59 59.6	40.462	139.102	Japan Sea	7 7	PMO, VAH, RUV
27	1985 03 03	22:47 06.9	-33.155	-71.980	Chile	7 8	PMO VAH, RUV

* Event numeration starts at 20 to avoid confusion with data from Paper I.

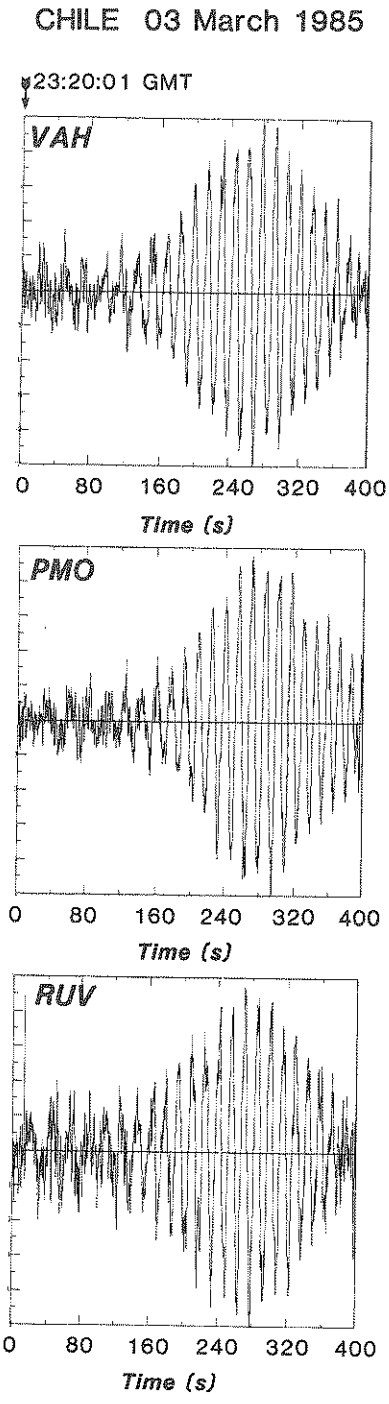

Figure 8. Example of Rayleigh-wave vertical seismograms from short-period instruments. 1985 Chilean event recorded across the Rangiroa array.

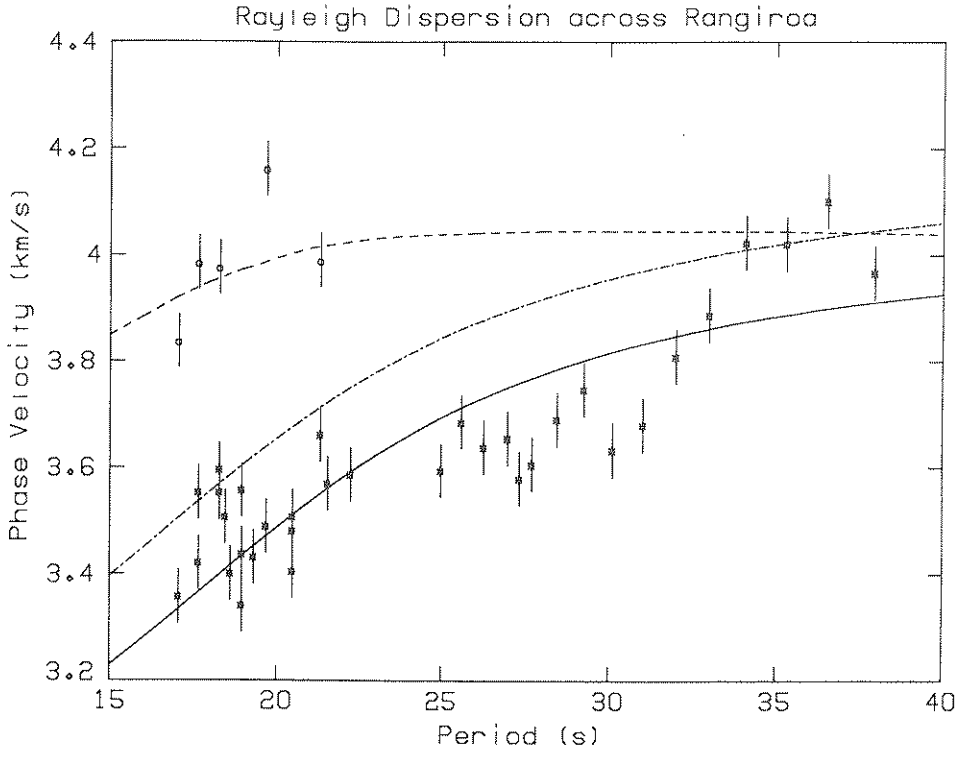

Figure 9. Rayleigh wave dispersion across Rangiroa and Tahiti. The symbols (with ±0.05 km s^{-1} error bars) are individual phase velocities measured across the Rangiroa (asterisks) and Tahiti (circles) short-period subarrays. The various lines are theoretical dispersion models: dashed line: Oceanic Model 3 (Mitchell & Yu 1980); dashed–dot line: Poisson solids with *P*-velocities given for Rangiroa in Table 4; solid line: final shear velocity obtained from inversion (Model 4; Table 8).

The resulting phase velocities are plotted on Fig. 9. It is at once evident that the dispersion characteristics of Tahiti and Rangiroa differ considerably, the latter being, as expected, much slower than Tahiti. The dashed line on Fig. 9 shows a theoretical dispersion curve obtained for Mitchell & Yu's (1980) Model 3 adequate for oceanic structures of 50–100 Myr in age. The dash–dot line on Fig. 9 is for a Tuamotu model featuring the layering obtained in Section 1, under the assumption of a constant Poisson ratio $\nu = 1/4$, and with reasonable values of the densities of the various oceanic layers. While the few data points available for the Tahiti–Mehetia array are in general agreement with this model, dispersion across Rangiroa is 0.25–0.40 km s^{-1} slower than the average oceanic model in the 17–35 s range. This confirms the fundamentally different structure of the two islands.

Two-station method, Tuamotu plateau; a correction to Paper I

In Paper I, we investigated the Rayleigh dispersion over the Tuamotu archipelago by using exclusively the relatively long path TPT–RKT (1606 km). Unfortunately, in selecting the few events which could be used with the two-station method, we assigned a maximum difference in azimuth of 5° at the epicentre between the two stations involved. In most cases when the two-station method is used, the major concern is the elimination of any possible variation in source phase with azimuth, so that this margin is indeed safe. *This is because it is tacitly assumed that the structures studied have wavelengths much greater than the*

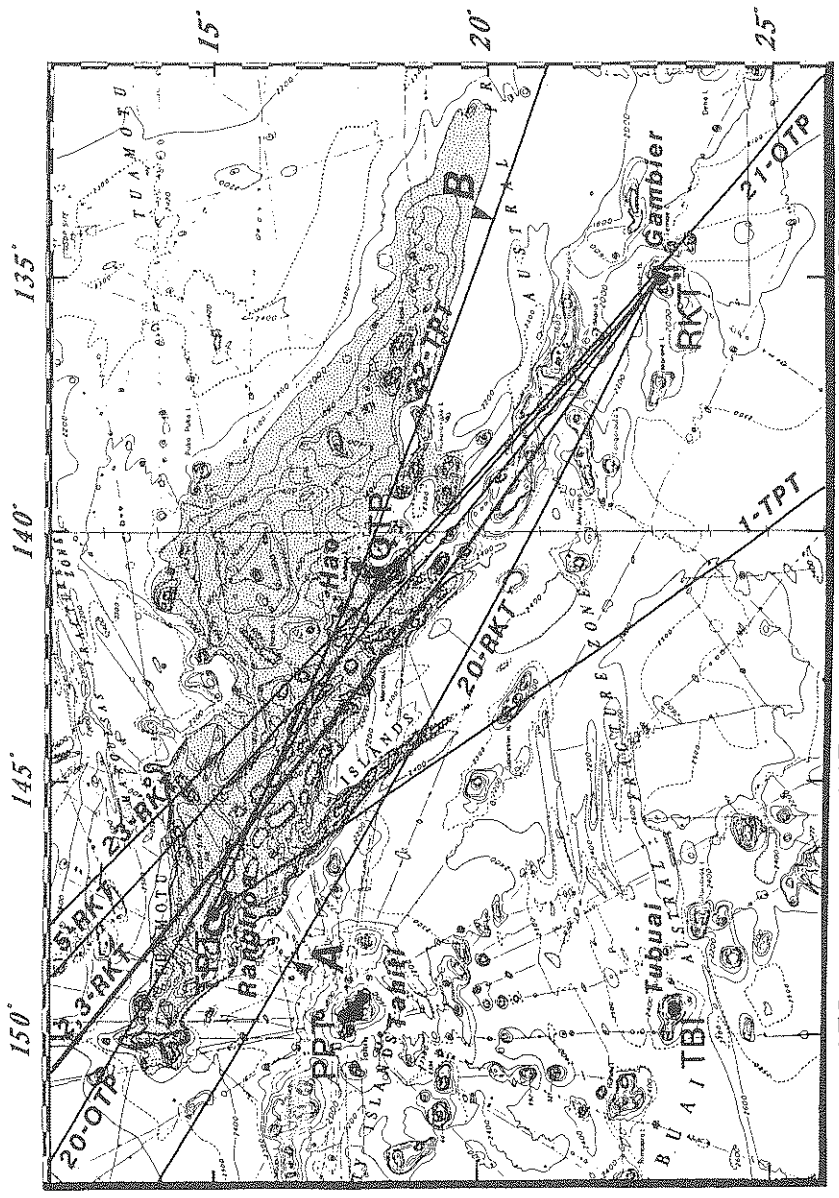

Figure 10. Location map of the Rayleigh wave dispersion experiments in the Tuamotu–Gambier area (Paper I and this study). The shaded area is the Tuamotu plateau, identified by the continuous 2000 fathom isobath (Mammerickx *et al.* 1975). Full dots identify long-period stations, with three-letter codes; and the corresponding islands or atolls are emphasized and their full name also given. The solid lines are selected great circle arcs involved in the two-station experiments (e.g. Epicentre 1 to Tiputa). Arrows along rays 20-RKT and 22-TPT identify points A and B; see text for details.

maximum lateral distance between the two rays. In our particular case, this assumption can be violated by the Tuamotu plateau which is only 300 km in width. In addition, since Paper I was published, it has become evident that the structure along the great circle arc between RKT and TPT is itself heterogeneous, since islands along the southern branch of the Tuamotus (e.g. Maria, Tureia) are not totally compensated (Okal & Cazenave 1985), suggesting a thinner crust. While our phase velocity dataset as published in Fig. 3 and Table 3 of Paper I remains unaltered, it is incorrect to assign it to the Tuamotu plateau, since (i) some of the rays deviate substantially from the path RKT/TPT; and (ii) even that arc is not pure plateau in structure.

In the present paper, we study shorter paths by making use of station OTP, conveniently located half-way between TPT and RKT (TPT–OTP = 803 km; OTP–RKT = 828 km). In addition, we use earthquakes for which the alignment of the two stations with the epicentre is much improved, with a maximum difference in azimuth at the source of only 0.48°. Specifically, for Event 20, the great circle to OTP misses TPT by only 26 km; for Event 22, the ray to TPT misses OTP by 50 km (Fig. 10). These values are considerably less than the lateral extent of the plateau, and indeed shorter than the typical Rayleigh wavelength (80 km). Furthermore, as shown on Fig. 10, the Tuamotu plateau is continuous along the whole great circle arc TPT–OTP. Therefore, we take the results of this experiment as representative of the dispersion along the Tuamotu structure. Another advantage of this short path is that it eliminates all indeterminacy on the unknown integer part N of the phase shift between the two stations (see Paper I, equation 7, p. 723). Our results are given in Table 7(a) and Fig. 11. We find that the dispersion is actually *slower* than predicted by an average oceanic model of adequate age, such as Mitchell & Yu's (1980). This is especially true at the higher frequencies, in general agreement with the thicker crust revealed by the refraction experiment.

In addition, we used Events 21 and 23 to study the path OTP–RKT. Here again, and as shown on Fig. 10, we achieved excellent alignments, with source azimuth differences of at most 0.11°; the great circle from Event 21 to OTP misses RKT by only 9 km, and that from Event 23 to RKT misses OTP by 10 km. Phase velocities along this path, listed in the second group of columns in Table 7(a), are found to be slightly faster than along TPT–OTP. This is in general agreement with the fact that it samples some uncompensated structures, such as Tureia, which most probably involve thinner crust than does a genuine piece of Tuamotu plateau.

Finally, we used the TPT and RKT records from Events 20 and 22 to attempt a study of the whole path TPT–RKT, and a comparison with the results of Paper I. The spectral characteristics of these two events are quite different, and a direct comparison between them is difficult; nevertheless, the last two columns of Table 7(a) clearly show strikingly different behaviour: phase velocities obtained from Event 22 are comparable to, or somewhat slower than, along TPT–OTP; results from Event 20 are significantly faster than along TPT–OTP and RKT–OTP. A simple explanation can be found on Fig. 10: because of the relatively poor alignment of the stations with the epicentre (respectively 1.69° and 3.65° at the source), this two-station experiment is actually ill-conceived; assuming that no other anomalous structures exist on the paths from the seismic sources to the Tuamotu–Gambier region, results from Event 20 are actually representative of the path Point A–RKT, which misses the plateau totally, while those from Event 22 cover the path Point B–TPT, which samples at least 1000 km of the plateau, and possibly interacts with the prolongation of its northern branch to the Austral Fracture Zone over an additional 700 km. This experiment clearly shows the extreme sensitivity of two-station analyses to local structure and imperfect alignment, and warrants a careful re-interpretation of the original data in Paper I.

Table 7a. Dispersion of Rayleigh waves in the Tuamotu–Gambier area. New results from this study.

Period (s)	Phase Velocity (km/s)							
	TPT-OTP			OTP-RKT			"TPT-RKT"	
	Event 20	Event 22	Mean	Event 21	Event 23	Mean	Event 20	Event 22
15.06				3.730		3.730		
15.52				3.779		3.779		
16.00								
16.52				3.739		3.739		
17.07				3.800		3.800		
17.66				3.824		3.824		
18.29	3.790		3.790	3.834		3.834	3.952	
18.62	3.784		3.784					
18.96	3.807		3.807	3.822		3.822	3.927	
19.32	3.819		3.819					
19.69	3.825	3.822	3.824±0.00	3.840		3.840	3.922	
20.08	3.850		3.850					
20.48	3.883	3.839	3.861±0.03	3.831		3.831	3.933	
20.90	3.883		3.883					
21.33	3.866	3.861	3.864±0.00	3.878	3.938	3.908±0.04	3.940	
21.79	3.879		3.879					
22.26	3.891	3.873	3.882±0.01		3.941	3.941		
22.76	3.886		3.886					
23.27	3.879	3.873	3.876±0.00		3.969	3.969		
23.81	3.856		3.856					
24.38	3.861	3.892	3.877±0.02		3.959	3.959		
24.98	3.873		3.873					
25.60	3.902	3.905	3.904±0.00					
26.26	3.913		3.913					3.947
26.95	3.869	3.909	3.889±0.03		3.944	3.944		3.940
28.44	3.849	3.912	3.881±0.04				3.999	3.942
29.26	3.902		3.902					
30.12							4.018	3.921
31.03	3.864		3.864					
32.00	3.898	3.936	3.917±0.03				4.038	3.901
33.03	3.934		3.934					
34.13		3.946	3.946					3.905
36.57		3.954	3.954					3.898
39.38		3.944	3.944					3.889
42.67		3.941	3.941					
46.55		3.968	3.968					
51.20		3.985	3.985					
56.89		3.993	3.993					
64.00		4.030	4.030					
73.14		3.984	3.984					
85.33		3.986	3.986					
102.40		4.069	4.069					

Re-interpretation of the 'TPT–RKT' results of Paper I

Table 7(b) presents a recompilation of the dispersion obtained in Paper I from the two-station method applied between TPT and RKT. We also include our results from outside the chain using the event at Epicentre 10. In Paper I, we computed the dispersion between TPT and RKT for four earthquakes (Events 1–3 and 5, Table 2 of Paper I; Event 4 contributed only marginal data, for $T > 120$ s). For each of these events, we have plotted on Fig. 10 the actual great circle path of the longer of the two rays involved. It is immediately apparent that the rays from Event 1 to TPT travel at most 200 km over the plateau (the

Table 7b. Dispersion of Rayleigh waves in the Tuamotu–Gambier area. Re-interpretation of Paper I data.

Period (s)	Phase Velocity (km/s)					
	"TPT-RKT"					RKT-PPT
	Event 2	Event 3	Event 5	Mean	Event 1	Event 10
16.00					3.795	
16.52					3.825	
17.07					3.845	3.906
17.66					3.862	3.919
18.29					3.882	3.936
18.96			4.034	4.034	3.904	3.944
19.69			4.036	4.036	3.922	3.935
20.48			4.048	4.048	3.926	3.958
21.33			4.048	4.048	3.940	3.967
22.26			4.046	4.046	3.954	3.955
23.27			4.046	4.046	3.974	3.991
24.38			4.097	4.097	4.008	4.001
25.60	4.059	4.054	4.113	4.075±0.03	4.034	
26.95		4.042	4.141	4.091±0.07		
28.44		4.047	4.144	4.095±0.07		
30.12		4.081	4.139	4.110±0.04		
32.00	4.094	4.111	4.132	4.112±0.02		
34.13	4.071	4.112	4.134	4.106±0.03		
36.57	4.088	4.098	4.103	4.096±0.01		
39.38	4.080	4.086	4.090	4.085±0.01		
42.67	4.084	4.082	4.064	4.077±0.01		
46.55	4.085	4.086	4.068	4.080±0.01		
51.20			4.057	4.057		
56.89			4.048	4.048		
64.00		4.083	4.051	4.067±0.02		
73.14		4.050	4.058	4.054±0.01		
85.33			4.049	4.049		
102.40	4.122	4.082	4.086	4.097±0.02		
128.00			4.187	4.187		
170.67			4.465	4.465		

shaded area on Fig. 9). In Table 7(b), we have separated the data from Event 1; they are clearly faster than TPT–OTP and OTP–RKT (see Table 7a), and very comparable to both RKT–PPT (Event 10; Paper I, and last column of Table 7a), and Point A–RKT (Event 20; see above). All three paths actually sample genuine oceanic lithosphere; the slight slowness of the Event 1 data as compared with the RKT–PPT path would fit the expected anisotropy reported in Paper I, but is not significant given the precision of the data.

The situation with Events 2, 3, and 5 is rather complex. Application of the two-station method between TPT and RKT for these events yields values significantly faster (by 0.10–0.15 km s^{-1}) than along either TPT–OTP or OTP–RKT. Because these faster velocities are observed continuously over a large frequency range (0.01–0.05 Hz), they cannot possibly be an artifact of an erroneous choice of the integer part of the phase difference, N. Rather, Fig. 10 suggests that rays to TPT are slowed down by travelling at least 370 km over the plateau structure *before* reaching TPT, while rays to RKT, 80 km to the north, avoid it. This effect results in an apparent increase in phase velocity when measured by the two-station method; as observed in the data, it is more pronounced for Event 5, where the alignment is poorer.

However, it cannot by itself explain the entire discrepancy of 0.10–0.15 km s^{-1}, suggesting that additional, non-geometrical, effects take place, probably in the form of multipathing.

Among the other paths studied in Paper I, only the path TBI–OTP interacts with the Tuamotu structure, but only for a distance of 100 km, and at right angles to its general direction. Nevertheless, we further re-examined our whole dataset from Paper I, including the paths TBI–OTP, TBI–RKT, and RKT–Event 10–PPT. Because all these paths are substantially shorter than TPT–RKT, the choice of N along them is totally unambiguous, and our original interpretations cannot be altered. Since in Paper I we had recognized the Tuamotu structure as clearly anomalous, and based our comparisons with published models exclusively on the genuinely oceanic paths OTP–TBI, RKT–TBI, and PPT–Event 10–RKT, our mistaken interpretations along TPT–RKT *do not affect either any of our conclusions regarding applicability of pure-path models, or our whole discussion concerning the existence and orientation of azimuthal anisotropy*. Our description of the beating patterns observed at PPT for South Chilean earthquakes (Section 4 of Paper I), and the synthetic experiment are practically unchanged; since the dispersion is actually slower along the Tuamotu plateau, the origin and mechanism of the multipathing have to be more complex than proposed in Paper I.

INVERSIONS

In this section, we use inversion theory to obtain a number of constraints on the structure of Rangiroa and the Tuamotu Islands from our datasets of Rayleigh wave phase velocities.

Rangiroa

In the case of Rangiroa, we use a dataset consisting of the experimental dispersion curve of Fig. 9, between periods of 15 and 40 s, smoothed by a running average using 4 points in the frequency domain. Because of this small period range, our resolution is limited, and as a first step, we restrict ourselves to models consisting of three layers over a half-space, and invert only for the Layer 3 and mantle shear velocities. The thicknesses of the various layers is fixed during the inversion, but we carry out the inversions for various thicknesses of Layer 3, ranging from 10 to 35 km.

Since we solve only for the two unknown shear velocities, the problem, as posed, is strongly overdetermined. In order to preserve the stability of the solution, we replace the standard generalized inverse problem of minimizing

$$|\mathbf{Ax} - \mathbf{d}|^2, \tag{5}$$

where $\mathbf{d}$ is the data vector, $\mathbf{x}$ the sought parameter vector, and $\mathbf{A}$ the model matrix, with that of minimizing

$$(1 - \epsilon) \cdot |\mathbf{Ax} - \mathbf{d}|^2 + \epsilon \cdot |\mathbf{x}|^2. \tag{6}$$

This classic procedure (e.g. Aki & Richards 1980) has the effect of a compromise between resolution and stability, and guards against solutions varying strongly with slight fluctuations in the data. After several trials, we opted for $\epsilon = 0.1$, providing 90 per cent resolution and 10 per cent stability; we found that this number was sufficient to achieve good stability in all cases. The programme usually converged to 3 significant digits in 3 or 4 iterations. Results of the inversions are listed in Table 8. Because of the limited resolution, there is an obvious trade-off between the depth to the Moho and the shear velocities at depth. In general, the root mean squares (r.m.s.) residual σ decreases regularly with increasing depth. This is simply

an expression of the substantial dispersion exhibited by the data between 15 and 40 s, a feature difficult to model with a shallow structure, for which the dispersion has already flattened to its asymptotic values at these periods (see dashed line on Fig. 9). For crustal depths greater than 30 km, σ becomes comparable to the uncertainty in the data, and as a result the fit to the data ceases to be significantly improved by an increase in depth.

From the *P*-wave velocities independently constrained by the refraction data, we computed the resulting Poisson ratios ν, and list them in the last two columns of Table 8. For thicknesses of Layer 3 of 20 km or less, the values of ν required by the Rayleigh inversion become unrealistically large: any $\nu > 0.30$ would require either an eclogitic composition, or large amounts of partial melting in the crust; our shallowest model would give it mechanical properties similar to those of the inner core! We reject all such models, and constrain the crust to be at least 30 km deep.

Table 8. Results of inversion of Rangiroa Rayleigh dispersion.

Model Number	Thickness of Layer 3	Depth to Moho	Inverted *S*-wave velocities (km/s)		r.m.s residual σ	V_P/V_S		Poisson ratio ν	
	(km)	(km)	Layer 3	Mantle	(km/s)	Layer 3	Mantle	Layer 3	Mantle
1	10	16.8	2.589	4.357	0.0973	2.638	1.859	0.42	0.30
2	15	21.8	3.183	4.390	0.0733	2.146	1.845	0.36	0.29
3	20	26.8	3.510	4.444	0.0544	1.946	1.823	0.32	0.28
4	24.5	31.3	3.687	4.493	0.0413	1.852	1.803	0.29	0.28
5	30	36.8	3.826	4.563	0.0305	1.785	1.775	0.27	0.27
6	35	41.8	3.909	4.638	0.0268	1.747	1.746	0.26	0.26

In order to further investigate this result, we ran a few inversions with a larger number of layers, in an attempt to force resolution of the lower structure of the crust. Specifically, we used a model of eight layers over a half-space, with 5 km-thick layering from 20.8 to 40.8 km depth, and solved for the five deepest shear velocities, with the same starting models as before, featuring initial Mohos at various depths. For initial Moho depths of 30.8 km or greater, the inversion does not significantly move the discontinuity. For an initial Moho depth of 22 km, the inversion moves it down 20 km, and produces a model very similar to our thickest three-layer result (Model 6, Table 8). For an initial Moho depth of 27 km, the inversion produces a strong low-velocity zone between 32 and 42 km, and a strong discontinuity at 42 km; none of these models improves significantly the goodness of fit with respect to our thick three-layer models; this expresses the relative lack of resolution of our data. We conclude that the data cannot be fit significantly better than by a model with three crustal layers, a depth to the Moho of 31 km, and shear velocities of 3.69 km s^{-1} in Layer 3 and 4.49 km s^{-1} in the mantle (Model 4, Table 8). Models with a thicker crust, and larger velocities are also acceptable (Models 5 and 6). Models 1–3, featuring a thinner crust, are unacceptable, in view of the improbable Poisson ratios they would require.

Tuamotu plateau

In the case of the Tuamotu plateau, we use as a dataset the values in the fourth column of Table 7(a), interpolated every 5 s between 20 and 90 s. Because of the relatively low

Table 9. Results of inversion of Tuamotu Rayleigh dispersion.

Model Number	Thickness of Layer 3 (km)	Depth to Moho (km)	Inverted *S*-wave velocities (km/s)		r.m.s. residual σ (km/s)	V_P/V_S		Poisson ratio ν	
			Layer 3	Mantle		Layer 3	Mantle	Layer 3	Mantle
1	10.5	16.7	4.043	4.491	0.0382	1.694	1.804	0.23	0.28
2	15.5	21.7	3.979	4.533	0.0367	1.722	1.787	0.25	0.27
3	18.0	24.2	3.975	4.557	0.0346	1.723	1.777	0.25	0.27
4	20.5	26.7	4.004	4.585	0.0325	1.711	1.767	0.24	0.26
5	25.5	31.7	4.185	4.610	0.0297	1.637	1.757	0.20	0.26
6	30.5	36.7	4.307	4.635	0.0276	1.590	1.748	0.17	0.26
7	35.5	41.7	4.411	4.653	0.0258	1.553	1.741	0.15	0.25

resolution of the data, we proceed as in the case of Rangiroa: we use a model of five layers over a half-space, featuring a low-velocity zone between depths 90 and 185 km appropriate for the age of the lithosphere under the plateau (Mitchell & Yu 1979). As a first step, we solve only for the shear velocities in Layer 3 and the lid, for various depths to the Moho, as listed in Table 9. In general, r.m.s. residuals decrease slightly with increasing depth to the Moho; this loses significance around 30 km of crustal thickness when the r.m.s. residual

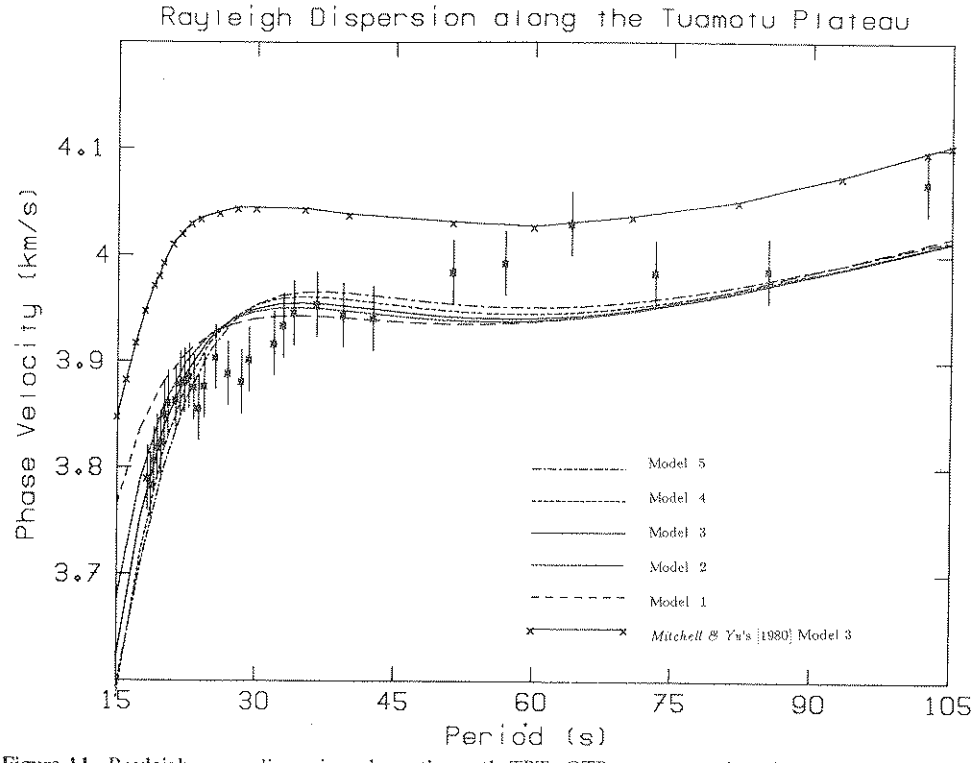

Figure 11. Rayleigh wave dispersion along the path TPT–OTP, representative of the Tuamotu plateau. Asterisks (with ±0.03 km s^{-1} error bars) are individual measurements (see Table 7a). The upper curve (with × symbols) is the theoretical dispersion for Mitchell & Yu's (1980) Model 3. The other curves are for various inverted models (see key and Table 9).

becomes comparable to the uncertainty in the data (0.03 km s^{-1}). Models 5–7 with a thicker crust can be rejected on the basis of the very low Poisson ratios required (with V_P determined from the results of Section 1): no material believed to make up the lower crust has Poisson ratios of 0.20 or less. Despite only marginal improvement of the overall fit to the dataset (as measured by the r.m.s. residual), Models 2–4 with crustal thicknesses of 21.7–26.7 km provide a better fit to the higher-frequency part of the dataset (20 and 25 s). Model 1, with the thinnest crust (16.7 km b.s.l. to the Moho, a typical 'Hawaiian' structure) clearly fails to account for the sharply reduced velocities at periods less than about 27 s (see Fig. 11). On this basis, we prefer Models 2–4, which provide a more balanced fit to the data throughout the frequency spectrum.

As in the case of Rangiroa, we also attempted a more general inversion by solving for the four shear velocities in Layer 3, the lid, the low-velocity zone, and the upper mantle half-space, for a variety of Moho depths. All solutions converge with an r.m.s. residual less than the data uncertainty (usually on the order of 0.015 km s^{-1}). However, models with a shallow Moho (less than 22 km b.s.l.) lead to a total disappearance of the low-velocity channel, with very slow velocities both in the lid and upper mantle. These models would be impossible to reconcile with the neighbouring oceanic structures.

In conclusion, our surface wave results require a crust at least 31 km deep under the atoll of Rangiroa, and our preferred range of Moho depths under the plateau between Rangiroa and Hao is 22–27 km.

3 Discussion and conclusion

Both the seismic refraction experiments and the Rayleigh wave investigations indicate an extremely thick crust under the Tuamotu plateau in general, and Rangiroa in particular. Detailed refraction and gravity work under the Hawaiian Islands has revealed a thickening of the crust to only 16 km b.s.l., with a possible high density volcanic plug extending an additional 4 km under Oahu and Molokai (Watts *et al.* 1985). These values, and earlier ones ranging from 10 to 20 km below the Hawaiian chain (Furumoto *et al.* 1968; 1971) are in agreement with our results under Tahiti, but fall short of the values of crustal thickness reported here for Rangiroa. On the other hand, large crustal thicknesses (up to 42 km b.s.l.) have been reported under the Ontong–Java plateau (Furumoto *et al.* 1976), the Nazca Ridge (Cutler 1977), the Broken Ridge (Francis & Raitt 1967), the Shatsky Rise (Den *et al.* 1969), the Iceland–Færœ plateau (Bott & Gunnarsson 1980), and the Walvis Ridge (Goslin & Sibuet 1975; Chave 1979). All these edifices are believed to have formed 'on-ridge', i.e. in the immediate vicinity of an active spreading centre, with the thickening of the crust due to lack of elastic support from the young thin plate, resulting in total isostatic compensation (Detrick & Watts 1979). In the case of the Tuamotu Islands, our results support this general model, with the plateau being formed at the defunct Farallon Ridge.

This view is also supported by the small geoid signature of the plateau. Fig. 12 is a 3-D rendition of the *SEASAT* geoid data in the south-central Pacific. It is noteworthy that the Tuamotu plateau, one of the largest topographic features in the Pacific, displacing in excess of 10^6 km^3 of water has a generally negligible contribution to the geoid anomaly, as compared with the Society or Austral Islands (both less than 10^5 km^3). Only the south-eastern branch of the plateau, heading from Hao to Tureia and Marutea, and the Anaa finger protruding from its southern flank, are less than totally compensated.

The velocities obtained by refraction for the various layers of the crust are generally very comparable to those found elsewhere; in particular, our seismic section for the Tuamotus is in excellent agreement with the results of Furumoto *et al.* (1976) and Hussong *et al.* (1979)

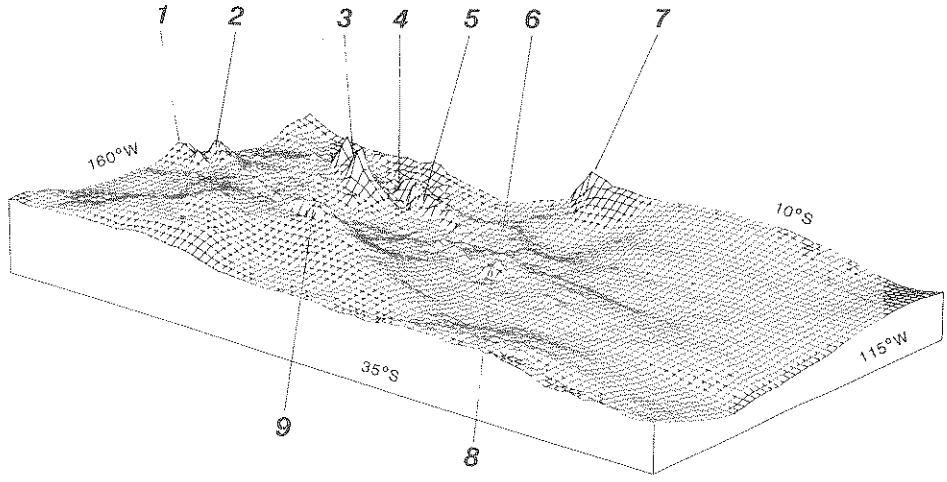

Figure 12. Three-dimensional map of the *SEASAT* geoid in French Polynesia (A. Cazenave, private communication). This is a view looking north-west through the area of the Society, Austral, Tuamotu and Gambier Islands. Principal features include (1) Rarotonga; (2) Lower Cook Islands; (3) Tahiti and Society Islands; (7) Marquesas Islands; (8) Mururoa–Gambier chain; and (9) Austral Islands. Among the Tuamotu Islands, only the southern finger extending through Anaa and to a lesser extent the southern branch from Hao to Tureia and the adjoining seamounts, show a weak geoid signature (5). On the other hand, the locations of Rangiroa (4) and the northern branch (6) show no geoid anomaly and must be fully compensated [see Okal & Cazenave (1985) for details].

in the Ontong–Java area, including the absence of (or failure to detect) lower crustal reflectors (Layer 3B). The mantle shear velocities obtained in our preferred models for Rangiroa (4.49 km s^{-1}) and the Tuamotus (4.55 ± 0.03 km s^{-1}) are somewhat slower than reported for old oceanic basins (4.70–4.80 km s^{-1}); they are more comparable to values found at oceanic ridges (Walker 1965; Walker & Sutton 1971; Hart & Press 1973), but do not reproduce the anomalously low values (4.26 km s^{-1}) obtained by Chave (1979) under the Walvis Ridge. The latter must have a regional origin.

Finally, we discuss the 2 km thickness of Layer 1′ at Rangiroa, which we interpret as a limestone cap of the volcanic edifice. This value is generally supported by preliminary results of a geomagnetic survey at 3309 points in and around the atoll (K. Yaskawa, private communication), which suggests a carbonate structure 1800 m thick. Furthermore, deep drilling at Enewetak and Bikini atolls (Schlanger *et al.* 1963) has revealed basement at 1400 and 1300 m, respectively. Values of 350–400 m have been found at Mururoa and Fangataufa (Chevalier 1973), and drilling at DSDP sites 289 (Ontong–Java plateau) and 317 (Manihiki plateau) has reached basement at respectively 1271 and 647 m (Andrews *et al.* 1975a; Schlanger *et al.* 1976b).

The rates of subsidence necessary to build a 2 km limestone cap can be estimated as follows: the age of the Tuamotu plateau in the vicinity of Rangiroa is at least 52 Myr (but probably not much more) on the basis of redeposited reef fossils found in volcanogenic siltstones drilled 745 m below the seafloor at DSDP Site 318 (Schlanger *et al.* 1976a); the Rangiroa edifice has to be younger, but no other direct constraint on its age exists. An age of 50 Myr (a probable upper limit) for the atoll would require a limestone growth rate of 40 μm yr^{-1}, well within the generally accepted values of 10–100 μm yr^{-1} for the tectonic subsidence of oceanic basins (Watts & Ryan 1976; Schlager 1981). Ages less than 20 Myr would require unacceptably fast growth rates, but can probably be ruled out anyway on the

basis of the negligible geoid signature of the atoll. Thus, the thickness of the limestone cap on Rangiroa, although large, is not unreasonable.

In conclusion, our seismic investigations, both through refraction and surface wave methods, prove that the Tuamotu Plateau, and in particular Rangiroa atoll, have very thick crust, extending to 31 km b.s.l. This makes them comparable to such structures as the Ontong–Java plateau or the Iceland–Færœ Ridge, and supports the idea that they formed 'on-ridge' and are fully compensated. While these results agree with those of previous experiments conducted by remote sensing (e.g. *SEASAT* studies), they provide the first *in situ* geophysical investigation of this large and important Pacific Ocean structure.

Acknowledgments

We thank the French Navy for the logistics and execution of the seismic refraction campaign, Anny Cazenave for collaboration over the *SEASAT* data and for a preprint, and Professor K. Yaskawa for preliminary results of his geomagnetic sounding of Rangiroa. Discussions with Craig Bina on the mineralogical significance of Poisson ratios, and with Sy Schlanger on many aspects of Pacific islands geology, are gratefully acknowledged. The paper was improved by the comments of Donald Hussong and another reviewer. This research was supported by Commissariat à l'Energie Atomique (France), and the Office of Naval Research, under Contract N00014-84-C-0616.

References

Aki, K. & Richards, P. G., 1980. *Quantitative Seismology*, W. H. Freeman and Co., San Francisco.

Alexander, S. S., 1963. Surface-wave propagation in the western United States, *PhD thesis*, California Institute of Technology, Pasadena.

Andrews, J. E., Packham, G., Eade, J. V., Holdsworth, B. K., Jones, D. L., Klein, G. deV., Kroenke, L. W., Saito, T., Shafik, S., Stoeser, D. B. & van der Lingen, G. J., 1975. Site 289, *Initial Reports of the Deep-Sea Drilling Project*, 30, pp. 231–398, Washington DC, US Govt. Printing Office.

Bott, M. H. P. & Gunnarsson, K., 1980. Crustal structure of the Iceland–Færœ Ridge, *Geophys. J.*, 47, 221–227.

Calmant, S. & Cazenave, A., 1985. The elastic lithosphere under the Cook–Austral and Society Islands, *Earth planet. Sci. Lett.*, 77, 187–202.

Chave, A. D., 1979. Lithospheric structure of the Walvis Ridge from Rayleigh wave dispersion, *J. geophys. Res.*, 84, 6840–6848.

Chevalier, J.-P., 1973. Geomorphology and geology of coral reefs in French Polynesia, in *Biology and Geology of Coral Reefs*, Vol. 1: *Geology 1*, pp. 113–141, eds Jones, O. A. & Endean, R., Academic Press, New York.

Cutler, S. T., 1977. Geophysical investigations of the Nazca Ridge, *MS thesis*, University of Hawaii, Honolulu.

Den, N., Ludwig, W. J., Murauchi, S., Ewing, J. I., Hotta, H., Edgar, N. T., Yoshii, T., Kubotera, A., Asanuma, T., Hagiwara, K., Sato, T. & Ando, S., 1969. Seismic refraction measurements in the northwest Pacific, *J. geophys. Res.*, 74, 1421–1434.

Detrick, R. S. & Watts, A. B., 1979. An analysis of isostasy in the world's oceans, 3. Aseismic ridges, *J. geophys. Res.*, 84, 3637–3653.

Fischer, K. M., McNutt, M. K. & Shure, L., 1987. Thermal and mechanical constraints on the lithosphere beneath the Marquesas swell, *Nature*, in press.

Forsyth, D. W., 1975. The early structural evolution and anisotropy of the oceanic upper mantle, *Geophys. J. R. astr. Soc.*, 43, 103–162.

Francis, T. J. G. & Raitt, R. W., 1967. Seismic refraction measurements in the southern Indian Ocean, *J. geophys. Res.*, 72, 3015–3041.

Furumoto, A. S., Woollard, G. P., Campbell, J. F. & Hussong, D. M., 1968. Variations in the thickness of the crust in the Hawaiian archipelago, in *The Crust and Upper Mantle of the Pacific Area, Geophys. Monog.*, 12, pp. 94–111, Am. Geophys. Un., Washington, DC.

Furumoto, A. S., Campbell, J. F. & Hussong, D. M., 1971. Seismic refraction surveys along the Hawaiian Ridge, Kauai to Midway, *Bull. seism. Soc. Am.*, **61**, 147–166.

Furumoto, A. S., Webb, J. P., Odegard, M. E. & Hussong, D. M., 1976. Seismic studies on the Ontong–Java plateau, 1970, *Tectonophysics*, **34**, 71–90.

Gordon, R. G. & Henderson, L. J., 1987. Pacific plate hot spot tracks, *J. geophys. Res.*, in press.

Goslin, J. & Sibuet, J. C., 1975. Geophysical study of the easternmost Walvis Ridge, South Atlantic: deep structure, *Bull. geol. Soc. Am.*, **86**, 1713–1724.

Grall, H. M., Hanan, B., Okal, E. A. & Schilling, J.-G., 1985. The Macdonald hotspot: Pb isotopes (abstract), *Eos, Trans. Am. Geophys. Un.*, **66**, 409.

Hadley, D. M. & Kanamori, H., 1979. Regional *S*-wave structure for southern California from the analysis of teleseismic Rayleigh waves, *Geophys. J. R. astr. Soc.*, **58**, 655–666.

Hart, R. S. & Press, F., 1973. S_n velocities and the composition of the lithosphere in the regionalized Atlantic, *J. geophys. Res.*, **78**, 401–411.

Hussong, D., Wipperman, L. & Kroenke, L., 1979. The crustal structure of the Ontong–Java and Manihiki oceanic plateaux, *J. geophsy. Res.*, **84**, 6003–6010.

Institut Géographique National, 1969. *Carte de l'Océanie Française au 1/2000000 (Iles de la Société–Iles Tubuai)*, Paris.

Jarrard, R. & Clague, D. A., 1977. Implications of Pacific island and seamount ages for the origin of volcanic chains, *Rev. Geophys. Space Phys.*, **15**, 57–76.

Kanamori, H. & Anderson, D. L., 1977. Importance of physical dispersion in surface wave and free oscillation problems: review, *Rev. Geophys. Space Phys.*, **15**, 105–112.

Mitchell, B. J. & Yu, G.-K., 1980. Surface-wave dispersion, regionalized velocity models, and anisotropy of the Pacific crust and upper mantle, *Geophys. J. R. astr. Soc.*, **63**, 497–514.

Morris, G. B., Raitt, R. W. & Shor, G. G. Jr, 1969. Velocity anisotropy and delay-time maps of the mantle near Hawaii, *J. geophys. Res.*, **74**, 4300–4316.

Okal, E. A., 1977. The effect of intrinsic oceanic upper-mantle heterogeneity on the regionalization of long-period Rayleigh wave phase velocities, *Geophys. J. R. astr. Soc.*, **49**, 357–370.

Okal, E. A. & Cazenave, A., 1985. A model for the plate tectonics evolution of the eastcentral Pacific based on *SEASAT* investigations, *Earth planet. Sci. Lett.*, **72**, 99–116.

Okal, E. A. & Talandier, J., 1980. Rayleigh wave dispersion in French Polynesia, *Geophys. J. R. astr. Soc.*, **63**, 719–733.

Okal, E. A., Talandier, J., Sverdrup, K. A. & Jordan, T. H., 1980. Seismicity and tectonic stress in the southcentral Pacific, *J. geophys. Res.*, **85**, 6479–6495.

Pilger, R. H., Jr, & Handschumacher, D. W., 1981. The fixed hotspot hypothesis and origin of the Easter–Sala y Gomez–Nazca trace, *Bull. geol. Soc. Am.*, **92**, 437–446.

Press, F., 1956. Determination of crustal structure from phase velocity of Rayleigh waves, Part I: Southern California, *Bull. geol. Soc. Am.*, **67**, 1647–1658.

Raitt, R. W., 1963. The crustal rocks in *The Sea*, Vol. 3, pp. 85–102, ed. Hill, M. N., John Wiley & Sons, New York.

Schlager, W., 1981. The paradox of drowned reefs and carbonate platforms, *Bull. geol. Soc. Am.*, **92**, 197–211.

Schlanger, S. O., Graf, D. L., Goldsmith, J. R., Macdonald, G. A., Sackett, W. M. & Portratz, H. A., 1963. Subsurface geology of Eniwetok Atoll, *US Geol. Survey Prof. Pap.*, **260-BB**, 991–1066.

Schlanger, S. O., Jackson, E. D., Boyce, R. E., Cook, H. E., Jenkins, H. C., Johnson, D. A., Kaneps, A. G., Kelts, K. R., Martini, E., McNulty, C. L. & Winterer, E. L., 1976a. Site 318, *Initial Reports of the Deep-Sea Drilling Project*, **33**, pp. 301–357, US Govt. Printing Office, Washington, DC.

Schlanger, S. O., Jackson, E. D., Boyce, R. E., Cook, H. E., Jenkins, H. C., Johnson, D. A., Kaneps, A. G., Kelts, K. R., Martini, E., McNulty, C. L. & Winterer, E. L., 1976b. Site 317, *Initial Reports of the Deep-Sea Drilling Project*, **33**, pp. 161–300, US Govt. Printing Office, Washington, DC.

Schlanger, S. O., Garcia, M. O., Keating, B. H., Naughton, J. J., Sager, W. W., Haggerty, J. A., Philpotts, J. A. & Duncan, R. A., 1984. Geology and geochronology of the Line Islands, *J. geophys. Res.*, **89**, 11261–11272.

Talandier, J. & Bouchon, M., 1979. Propagation of high-frequency P_n waves at great distances in the South Pacific and its implication for the structure of the lower lithosphere, *J. geophys. Res.*, **84**, 5613–5619.

Talandier, J. & Kuster, G. T., 1976. Seismicity and submarine volcanic activity in French Polynesia, *J. geophys. Res.*, **81**, 936–948.

Talandier, J. & Okal, E. A., 1984. The volcanoseismic swarms of 1981–1983 in the Tahiti–Mehetia area, French Polynesia, *J. geophys. Res.*, **89**, 11216–11234.

Walker, D. A., 1965. A study of the northwestern Pacific upper mantle, *Bull. seism. Soc. Am.*, **55**, 925–939.

Walker, D. A. & Sutton, G. H., 1971. Oceanic mantle phases recorded on hydrophones in the northwestern Pacific at distances between 9° and 40°, *Bull. seism. Soc. Am.*, **61**, 65–78.

Watts, A. B. & Ryan, W. B. F., 1976. Flexure of lithosphere and continental margin basins, *Tectonophysics*, **36**, 35–44.

Watts, A. B., ten Brink, U. S., Buhl, P. & Brocher, T. M., 1985. A multichannel seismic study of lithospheric flexure across the Hawaiian–Emperor seamount chain, *Nature*, **315**, 105–111.

Woollard, G. P., 1975. The interrelationships of crustal and upper mantle parameter values in the Pacific, *Rev. Geophys. Space Phys.*, **13**, 87–137.

Yu, G.-K. & Mitchell, B. J., 1979. Regionalized shear velocity models of the Pacific upper mantle observed from Love and Rayleigh wave dispersion, *Geophys. J. R. astr. Soc.*, **57**, 311–341.

Appendix 1

DESCRIPTION OF THE SOURCES IN THE SEISMIC REFRACTION EXPERIMENT

1. Refraction campaign of 1981–1982.

Sixty-six shots were fired along 4 seismic lines (see Fig. 2):

Numbers 1–4 south of Mehetia Island;

Numbers 5–12 and 73–74 along profile CD extending from north of Mehetia to north of Tahiti;

Numbers 63–72 along profile AB extending from Mehetia to the eastern shore of Tahiti;

Numbers 13–54 along profile AE from Mehetia to the southern shore of Rangiroa.

The sources consisted of 86-kg loads of TNT, dropped from shipboard and fired at a depth of 215 m. The precise timing of the explosion was detected by the ship's SONAR and radio transmitted to the central recording laboratory, and then corrected for the distance separating the SONAR antenna and the explosion site, as determined by onboard radar. The combination of the direct arrival and the first bottom-reflected one as recorded on the ship's SONAR was used to obtain a precise measurement of the water depth d at the source, whose knowledge is necessary for the computation of the water correction c_{ocean}. The exact location of the shots was estimated from the ship's astronomical navigation system, and improved by using T-wave arrival times at stations all over Polynesia; T-wave velocities have been previously determined to excellent accuracy. We estimate that all locations are known to better than 500 m.

2 Tahiti–Moorea–Mehetia campaign, 1966

Eight shots (numbers 75–82) fired along a line circling Tahiti and Moorea. The sources were 82-kg loads of TNT dropped from aircraft and fired at 40 m depth. Firing time detected by sonabuoys, radio transmitted to central laboratory.

3 Rangiroa campaign, 1968

Eight shots (numbers 55–62) were fired along profile FG east and west of Rangiroa. Same procedure as in 1966.

4 Tahiti and Moorea lagoons, 1963–64

Seven shots (numbers 83–89); loads varying from 30 to 80 kg TNT were dropped to the lagoon floors at depths of 30–40 m; firing was electrical with radio or telephone transmission to the central laboratory.

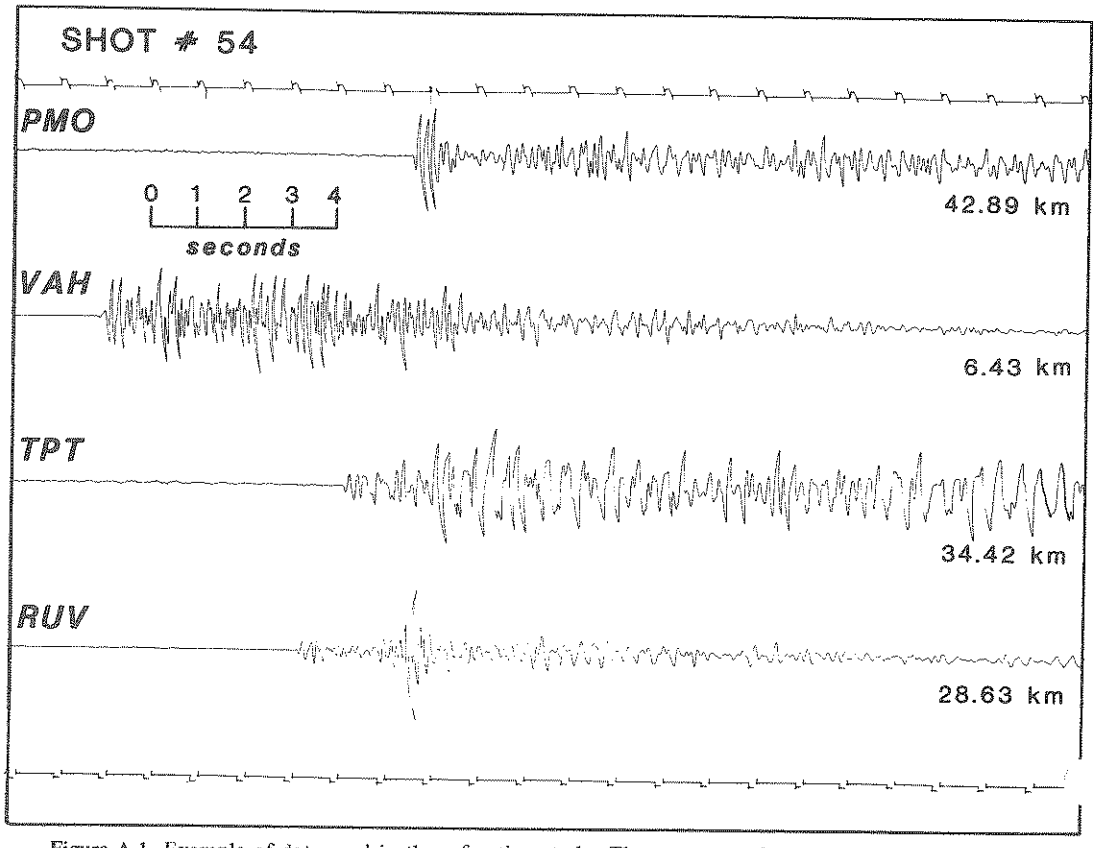

Figure A-1. Example of data used in the refraction study. These are records of shot number 54, fired at the extreme northern end of profile AE (see Fig. 2), and recorded at the Rangiroa array. Note the excellent signal/noise ratio, and the small time scale, allowing readings to be taken with a precision of ±0.05 s.

5 Rangiroa Lagoon, June 1982

Seven shots (numbers 90–96); loads from 1 to 20 kg TNT at floor depths of 10–20 m; electrical firing with radio transmission.

The complete dataset was recorded on magnetic tapes; arrival times were picked on hard copies played back at high speed with a variety of magnifications, and after applying high-pass filtering to eliminate the swell-generated background noise. The resulting response is flat in velocity between 2.5 and 16 Hz. An example of record used in the present study is given in Fig. A-1. We estimate the precision of the picks to be ±0.025 s.